



Article

Mapping Quaking Aspen Using Seasonal Sentinel-1 and Sentinel-2 Composite Imagery across the Southern Rockies, USA

Maxwell Cook 1,2,*, Teresa Chapman 3, Sarah Hart 4, Asha Paudel 4, and Jennifer Balch 5

- Department of Geography, University of Colorado Boulder, Boulder, CO 80309, USA
- Earth Lab, Cooperative Institute for Research in Environmental Sciences (CIRES), University of Colorado Boulder, Boulder, CO 80309, USA
- Chief Conservation Office, The Nature Conservancy, Fairfax, VA 22203, USA; tchapman@tnc.org
- Department of Forest and Rangeland Stewardship, Colorado State University, Fort Collins, CO 80523, USA; sarah.hart@colostate.edu (S.H.); paudelasha@gmail.com (A.P.)
- Environmental Data Science Innovation and Inclusion Lab (ESIIL), University of Colorado Boulder, Boulder, CO 80309, USA; jennifer.balch@colorado.edu
- * Correspondence: maxwell.cook@colorado.edu

Abstract: Quaking aspen is an important deciduous tree species across interior western U.S. forests. Existing maps of aspen distribution are based on Landsat imagery and often miss small stands (<0.09 ha or 30 m²), which rapidly regrow when managed or following disturbance. In this study, we present methods for deriving a new regional map of aspen forests using one year of Sentinel-1 (S1) and Sentinel-2 (S2) imagery in Google Earth Engine. Using observed annual phenology of aspen across the Southern Rockies and leveraging the frequent temporal resolution of S1 and S2, ecologically relevant seasonal imagery composites were developed. We derived spectral indices and radar textural features targeting the canopy structure, moisture, and chlorophyll content. Using spatial block cross-validation and Random Forests, we assessed the accuracy of different scenarios and selected the best-performing set of features for classification. Comparisons were then made with existing landcover products across the study region. The resulting map improves on existing products in both accuracy (0.93 average F1-score) and detection of smaller forest patches. These methods enable accurate mapping at spatial and temporal scales relevant to forest management for one of the most widely distributed tree species in North America.

Keywords: tree species classification; phenology; multi-temporal; random forest; Google Earth Engine



Citation: Cook, M.; Chapman, T.; Hart, S.; Paudel, A.; Balch, J. Mapping Quaking Aspen Using Seasonal Sentinel-1 and Sentinel-2 Composite Imagery across the Southern Rockies, USA. *Remote Sens.* **2024**, *16*, 1619. https://doi.org/10.3390/rs16091619

Academic Editor: Xiaodong Li

Received: 5 April 2024 Revised: 26 April 2024 Accepted: 28 April 2024 Published: 30 April 2024



Copyright: © 2024 by the authors. Licensee MDPI, Basel, Switzerland. This article is an open access article distributed under the terms and conditions of the Creative Commons Attribution (CC BY) license (https://creativecommons.org/licenses/by/4.0/).

1. Introduction

Across the interior western United States, quaking aspen (*Populus tremuloides Michx.*) is the dominant deciduous tree species in primarily mixed-conifer forests [1,2]. This important forest type provides ecosystem services, including biodiversity, wildlife habitat, recreational value, soil carbon sequestration, and vegetation recovery [1]. Aspens respond readily to canopy opening events (e.g., wildfire), and their persistence on the landscape is closely linked to disturbance type and periodicity [3–7]. Increasing synchronous disturbances (e.g., drought, bark beetle, and wildfire) may favor future dominance of quaking aspen in some regions [5,8,9]. However, a drier climate and altered disturbance regimes are likely to have varied impact on this foundational species across its range [10–13]. With growing focus on aspen ecology and management in the context of climate change and forest resiliency, production of high-resolution, accurate maps of its distribution at scales relevant to forest management activities is necessary.

Current nationwide maps of quaking aspen forest cover are developed using Landsat imagery at a 30 m spatial resolution, e.g., [14], and often fail to identify small stands, which offer prolific root suckering and expansion when managed or following disturbance [15,16]. There are three relevant 30 m maps of aspen distribution widely available for land managers

Remote Sens. 2024, 16, 1619 2 of 21

in the Southern Rockies and US: 1—the LANDFIRE Existing Vegetation Type (Landfire EVT) [14], 2—the United States Forest Service (USFS) National Individual Tree Species Parameter maps (USFS ITSP) [17], and 3—the USFS TreeMap [18]. Of these, only the Landfire EVT is provided in more than one time stamp. The remaining databases provide a snapshot in time as valuable baselines for managers. Collectively, these databases are limited in accuracy, their ability to detect small patches of aspen, and in their temporal range. For example, one of the more commonly used land cover maps in the US, the Landfire EVT, has an accuracy of 60–63% within aspen classes across the southwest US region for the 2016 remap product based on the product agreement assessment [19]. The USFS ITSP (c. 2014) and TreeMap (c. 2016) uniquely provide additional information from the USFS Forest Inventory and Analysis (FIA) plot data such as basal area and stem density but provide only a snapshot in time and have similar moderate accuracy for the aspen class. Developing new, higher-resolution maps will improve on these existing products at scales relevant to quaking aspen management.

Remote-sensing science has benefited in recent years from increasingly available free and open imagery and improved cloud-computing resources, facilitating the application of large-scale analysis of the Earth's surface [20,21]. In particular, the Sentinel missions, developed to support the Copernicus Programme and administered by the European Space Agency, have improved land use and landcover mapping efforts across broad geographic regions [22]. The Sentinel missions consist of a constellation of satellites carrying a range of sensors, including microwave (radar) and multispectral imaging. These data are made free and open to the public through the Copernicus Programme's free, full, and open data policy. Importantly, Sentinel products are also hosted in the Google Earth Engine (GEE) platform, which provides access to petabytes of earth systems data co-located with powerful cloud-computing resources [21].

The combination of spatial, spectral, and temporal resolutions of the Sentinel-2 (S2) Multispectral Instrument (MSI) is particularly useful for mapping vegetation with distinct phenological patterns [22]. Since 2015, S2 has provided global multispectral imagery at finer spatial (10–60 m), spectral (13-band), or temporal (5-day) resolutions compared to similar satellite missions such as Landsat (30–90 m, 4–8 bands, and 16-day) or Satellite Pour L'Observation de la Terre (1.5–6 m, 4-band, and 1–3 day). The four narrow red-edge bands captured by S2 improve species-level mapping, estimation of canopy chlorophyll content, and derivation of metrics such as gross primary productivity [23–26]. The 5-day temporal resolution increases availability of cloud-free images and facilitates analysis of land surface phenology and generation of seasonal cloud-free image composites [27]. Seasonal imagery improves species discrimination in forested regions, especially for deciduous types with distinct phenology [28–31].

However, as with any optical imagery, persistent cloud cover, haze, and snow cover are common issues affecting data acquisition and quality, especially for large-area image classification. In the case of vegetation mapping with multispectral imagery, multi-temporal image gap-filling can help overcome this challenge while retaining seasonal characteristics of the land surface [27]. Additionally, combining multispectral images with sensors less affected by atmospheric and environmental conditions, such as radar and microwave, can improve availability and quality of data.

Sentinel-1 (S1) collects cloud-penetrating synthetic-aperture radar (SAR) backscatter imagery at the same spatial and temporal resolution as S2, providing an important complementary data source for applications in land surface monitoring. As an active remote-sensing system, SAR measures the amplitude and phase of the backscatter signal, which corresponds to the physical properties (e.g., roughness) of the land surface [32]. In forested systems, the wavelength of radar signal emitted from the sensor determines the sensitivity and depth of penetration into the canopy [33]. S1 collects dual-polarized C-band SAR backscatter at a nominal frequency range, from 4 to 8 GHz (3.75–7.5 cm wavelength) in the microwave region of the electromagnetic spectrum. In this region, there is minimal pen-

Remote Sens. 2024, 16, 1619 3 of 21

etration into the forest canopy, making it useful for characterizing tree canopy roughness and texture [33,34].

Recent studies have shown potential for multi-temporal optical and radar (e.g., S1 and S2) imagery to improve vegetation mapping, especially in areas with persistent cloud cover and heterogeneous vegetation types [35–37]. The common spatial and temporal resolutions of S1 and S2 facilitate the use of these two data sources in tandem for classifying vegetation type [38,39]. Radar imagery is particularly useful in characterizing deciduous forest canopy structure during winter months when there is often persistent snow cover and/or cloud cover [35,36]. In deciduous forests specifically, the canopy structure changes at key phenological stages (e.g., onset of greenness increase, greenness maximum, onset of senescence, and greenness minimum), which may be characterized by multi-temporal S1 textural data, improving forest species classifications [27]. Furthermore, because SAR is sensitive to changes in the canopy roughness, textural features derived from backscatter imagery have improved classification of forest type [34,40]. Given the advances in classification accuracy using the Sentinel suite in a variety of recent studies, the efficacy in different ecosystems should be explored.

In this study, we have three primary objectives: (1) to develop methods for an open-source, accurate, and high-resolution (10 m) map of aspen cover across the Southern Rockies ecoregion (U.S. Environmental Protection Agency Level III) using combined S1 and S2 seasonal composite imagery with spectral indices and textural features; (2) to assess the agreement of this Sentinel-based map with existing 30 m products; and (3) to analyze and compare aspen patch size and total area across the Southern Rockies and within a targeted Colorado geography where aspen is currently a management focus. Finally, we provide results and data through a public interactive GEE application and make all code and methodology available in public repositories. We anticipate that a higher-resolution and more accurate map of aspen cover will facilitate targeted and effective management of aspen forests to increase the valued ecosystem services provided by this forest type.

2. Materials and Methods

For the classification of aspen forest cover in the Southern Rockies, over 5000 Sentinel-1 and Sentinel-2 images were acquired over one year (ca. 2019) from the GEE data catalog [21]. The mapping follows four primary steps (Figure 1). First, presence and background reference data were created using a combination of approaches (see Section 2.2). Second, Sentinel-1 and Sentinel-2 imagery was pre-processed, and seasonal median composites were generated based on key stages in the development of aspen forest canopies (see Section 2.3). Third, Random Forests were implemented with the presence and background reference data for the classification of Sentinel imagery composites (see Section 2.4). In this step, scenario testing was performed to identify the optimal combination of input features, and a spatial block cross-validation approach was used to assess model performance. The output from the classification model, a probability surface of aspen presence, was reclassified to aspen distribution based on an optimal probability threshold identified in model assessment. Finally, this new map of aspen distribution was compared with three existing products (see Section 2.5). This comparison included assessing accuracy of the validation reference data held out in model training, a pixel-based agreement between the products, and a comparison of landscape patch metrics.

2.1. Study Area

The Southern Rockies include portions of southern Wyoming, central and western Colorado, and northern New Mexico (Figure 2). Extending nearly 130k km², the elevation of the region ranges from approximately 1128 to 4268 m above sea level and is characterized by two major mountain belts and intermontane valleys and parks. While there is a mosaic of private and public protected lands, a large proportion of the region is federally managed (87.5%) including ten National Forests, two National Parks, and 57 federally listed wilderness areas [41]. There are a diverse array of ecosystem types including lower

Remote Sens. 2024, 16, 1619 4 of 21

montane/foothills, wet meadows, upper montane, subalpine, and alpine [42]. Forests cover approximately 64% (93.1k km²) of the landscape (Landfire EVT, ca. 2016; Figure 1), with quaking aspen serving as the dominant deciduous tree species (14.6% of forest cover) [14]. Quaking aspen persists on the landscape in both pure (stable) and mixed-conifer–aspen (seral) stands [4,43].

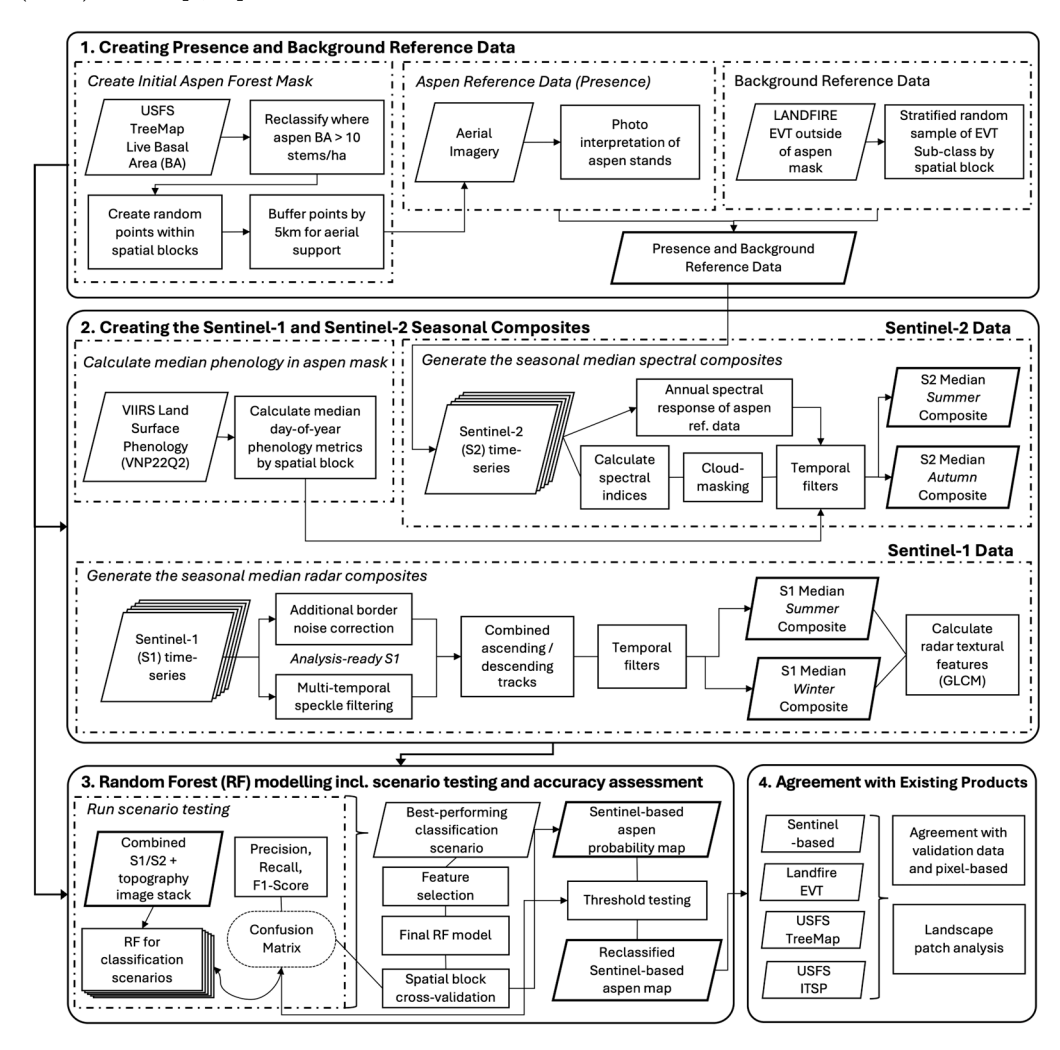


Figure 1. Workflow diagram of the data preparation and classification approach including four main steps: (1) creation of aspen reference data (presence) and background reference data; (2) creating the Sentinel-1 and Sentinel-2 seasonal imagery composites; (3) Random Forest classification including scenario testing, spatial block cross-validation, and creation of the final map product; and (4) assessment of the agreement between the Sentinel-based map of aspen forest cover and three existing products.

The study further evaluates results within a targeted geography in Colorado, the White River National Forest (NF), where quaking aspen is actively managed for multiple uses including wildlife habitat and wildfire risk reduction. The White River NF covers over 10,000 km² in central and western Colorado and is emblematic of the ecosystem types in the Southern Rockies. The region is also recreationally important, with 11 ski resorts, ten mountain peaks over 4267 m, and eight wilderness areas encompassing nearly a third of the total area. Aspen is dominant in this region, accounting for approximately 28% of forested lands (Landfire EVT, ca. 2016) [14]. The USFS manages both stable and seral stands of quaking aspen with aims to promote aspen regeneration in existing stands, improve wildlife habitat, and increase forest resilience to disturbance. Managers are using mechanical harvests (coppice silviculture) and prescribed fire to achieve these outcomes.

Large-area image classification presents unique challenges such as acquisition of representative training and validation data, collection of satellite imagery, and assessment

Remote Sens. 2024, 16, 1619 5 of 21

of model performance [20]. To overcome some of these challenges, we divided the Southern Rockies into 129 equal-area (50 km²) spatial blocks (Figure 2). These blocks provide an analytical unit to generate training and validation data (Section 2.2), imagery composites (Sections 2.3.1 and 2.3.2), and perform spatial block cross-validation during model training (Section 2.4).

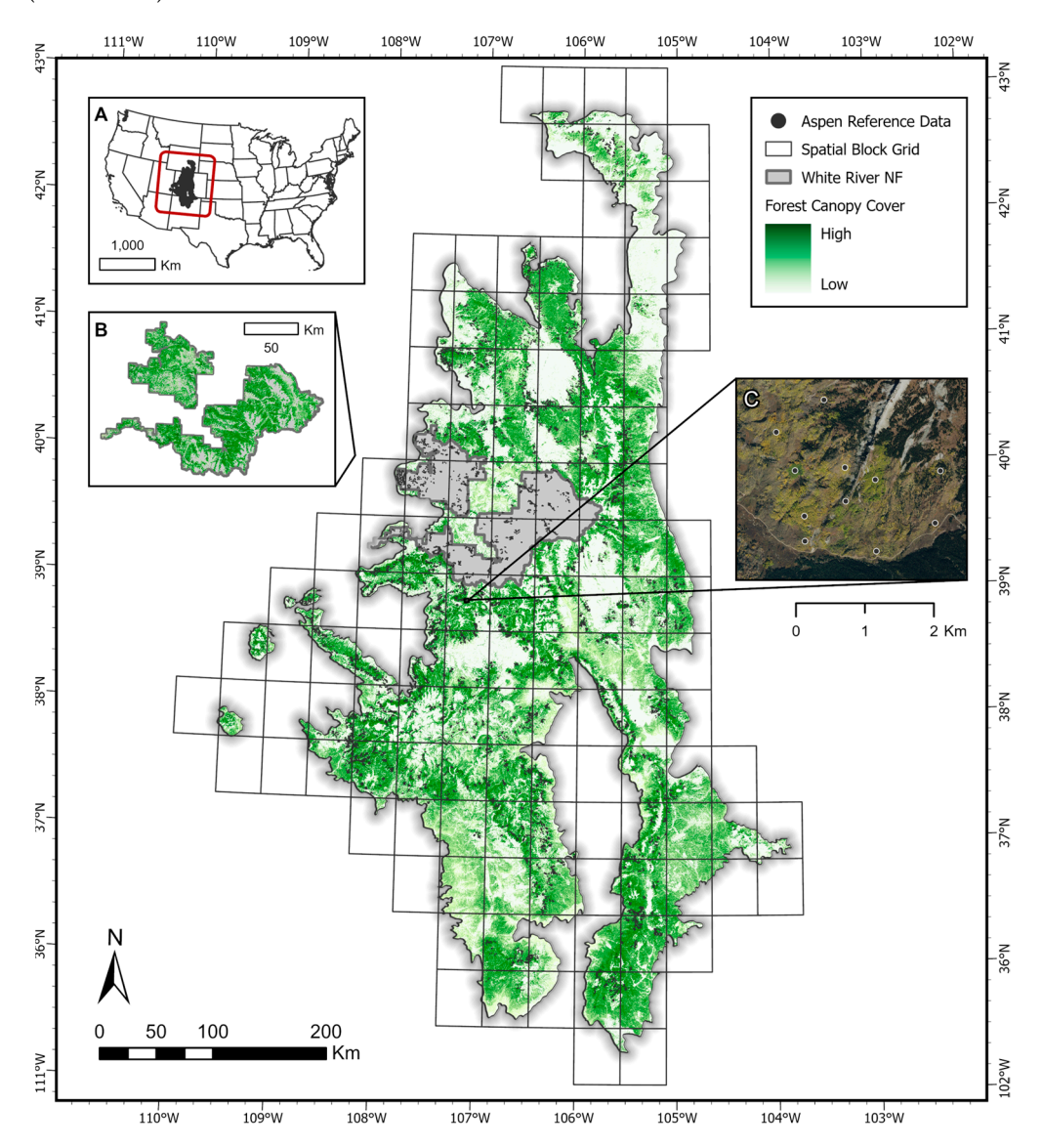


Figure 2. Map of the Southern Rockies showing the spatial block grid, case study landscape (White River NF), quaking aspen reference data (see Section 2.2) and forest cover (LANDFIRE Forest Canopy Cover, ca. 2016). Inset maps highlight (**A**) the location of the Southern Rockies in the western United States (**B**) the White River NF and forest canopy cover and (**C**) a reference area near Crested Butte, Colorado, showing aspen presence data with aerial imagery from the National Agricultural Imagery Program (NAIP, ca. 2017).

2.2. Reference Data

To train and validate classification models, we generated presence and background reference data. In binary classification, presence (i.e., positive class) represents the target land cover type or species, and background (i.e., negative class) captures a representative sample of all other cover types. This approach is particularly useful for applications where the desired result is a single land cover type or species and is commonly used in applications of habitat suitability modeling [44].

Remote Sens. 2024, 16, 1619 6 of 21

2.2.1. Quaking Aspen Reference Data

Availability of field-based measurements of aspen presence in the region is limited, particularly data aligned with Sentinel pixels. To overcome this challenge, aspen presence was determined using photo interpretation of high-resolution (1 m) aerial imagery from the United States Department of Agriculture (USDA) National Agricultural Imagery Program (NAIP, ca. 2017). A sampling design was implemented within areas of potential aspen presence (hereafter aspen mask), defined as pixels with a live aspen basal area greater than 10 stems/ha based on the USFS TreeMap product (ca. 2016) [18]. This threshold aligns with estimates for a potential minimum basal area in established aspen stands of the Southern Rockies [2]. For each spatial block, 10 spatially balanced random points were assigned inside the aspen mask and a 5 km buffer was applied as the spatial support to aid interpretation. An interpreter was trained to identify aspen from NAIP imagery and attempted to label a minimum of 10 pixels of aspen within the spatial support. If there were no obvious stands of aspen, a new random point was generated in the block. A random sample of was taken with a minimum distance of 100 m to limit effects of pseudoreplication. The resulting database includes 12,609 points across 95 spatial blocks.

2.2.2. Background Reference Data

Background reference data are representative of other major land cover types across the Southern Rockies and were derived from the Landfire EVT sub-class property (ca. 2016). To account for regional variation in cover types, proportional stratified samples were generated for each spatial block. The total number of samples in each block was set to ten times the number of presence points and divided amongst classes proportional to their area. A minimum sample size of 10 was set for each class in the block to ensure representation of minority classes, resulting in 73,031 samples across sub-classes (Table 1).

Table 1. Distribution of background samples from the Landfire EVT sub-class (ca. 2016). The number of samples represents the total across all spatial blocks with at least 100 presence points. We removed any classes which included quaking aspen forests.

Landfire EVT Sub-Class	Number of Samples
Evergreen closed tree canopy	23,957
Mixed evergreen-deciduous shrubland	13,421
Evergreen open tree canopy	12,991
Perennial graminoid grassland	7637
Annual graminoid/forb	3537
Evergreen shrubland	3273
Sparsely vegetated	2869
Mixed evergreen-deciduous open tree canopy	1016
Developed	896
Non-vegetated	808
Perennial graminoid	716
Evergreen dwarf-shrubland	669
Evergreen sparse tree canopy	624
Deciduous open tree canopy	617
Total	73,031

2.3. Satellite Imagery

One year (ca. 2019) of Sentinel-1 and Sentinel-2 imagery was collected in the GEE data catalog [21]. The collection and preparation of seasonal radar composites is described in Section 2.3.1, and optical imagery collection and compositing are described in Sections 2.3.2 and 2.3.4, respectively. In addition, we calculated spectral vegetation indices and radar textural features, which are described in Section 2.3.3.

Remote Sens. **2024**, 16, 1619 7 of 21

2.3.1. Sentinel-1

This study used winter (December–February) and summer (June–August) Sentinel-1 (S1) C-Band Ground Range Detected (GRD), which collects data in dual-polarization mode (VV and VH). These seasonal periods capture two distinct development stages of the forest canopy: peak greenness (summer) and dormancy (winter). The S1 collection was processed to analysis-ready data involving border noise correction and speckle filtering [45]. We combined both orbital passes (ascending and descending) for each polarization mode and calculated the median backscatter coefficient for the seasonal windows. In total, 556 individual S1 images were used to generate the median composites (324 for summer and 232 for winter).

2.3.2. Sentinel-2

All Sentinel-2 (S2) Multispectral Instrument (MSI) Level-2A surface reflectance scenes for the entire year across the Southern Rockies were initially collected (5137 tiles). Each surface reflectance tile includes four spectral bands at 10 m spatial resolution, six bands at 20 m, and three bands at 60 m. The 60 m bands (coastal aerosol, water vapor, SWIR-cirrus), which are uninformative for vegetation analysis, were excluded from the collection, and the remaining bands were resampled to a common 10 m spatial resolution (Table 2). Prior to generating seasonal composites (see Section 2.3.3), the annual spectral response for aspen presence was extracted from the full set of S2 tiles across the Southern Rockies for further analysis. In total, over 3000 images intersected the study area over the course of one year.

Table 2. Sentinel-1 and Sentinel-2 input features. All bands were resampled to a common spatial resolution of 10 m.

Satellite	Abbrev.	Name	Center Wavelength	Seasonal Windows
Sentinel-1	VV	Vertical–Vertical	5.5 cm	Summer/
	VH	Vertical-Horizontal	5.5 cm	Winter
Sentinel-2	B2	Blue	490 nm	
	В3	Green	560 nm	
	B4	Red	665 nm	
	B5	Red-edge 1	705 nm	
	В6	Red-edge 2	740 nm	Summer/
	B7	Red-edge 3	783 nm	Autumn
	B8	Near Infrared	842 nm	
	B8A	Red-edge 4	865 nm	
	B11	Shortwave Infrared 1	1610 nm	
	B12	Shortwave Infrared 2	2190 nm	

2.3.3. Additional Spectral and Textural Features

A suite of textural features and vegetation indices were derived from S1 and S2 imagery (Table 3). Given that radar backscatter is sensitive to canopy roughness, texture features may provide valuable information for discriminating forest types [34]. Specifically, the Gray Level Co-Occurrence Matrix (GLCM) derives textural features by assessing patterns of pixel intensities and spatial arrangement [40]. The derivatives of GLCM have been shown to improve land cover classifications from radar data [34,40,46]. We derived GLCM entropy, contrast, variance, and correlation using a 7×7 pixel neighborhood for winter and summer VH and VV polarization modes.

Six vegetation indices targeting forest canopy productivity, moisture, and chlorophyl content were derived from the S2 bands prior to generating seasonal composites. These included the Chlorophyll Index Red-edge (CIRE), Modified Chlorophyll Absorption in Reflectance Index (MCARI), Inverted Red-edge Chlorophyll Index (IRECI), Specific Leaf Area Vegetation Index (SLAVI), Modified Normalized Difference Water Index (MNDWI), and the Red-edge Normalized Difference Vegetation Index (NDVI705).

Remote Sens. 2024, 16, 1619 8 of 21

Table 3. Spectral vegetation indices and radar textural features. The formula and associated reference to calculate each index are provided where relevant. Indices and textural features were calculated for each seasonal window.

Satellite	Index	Abbreviation	Formula	Seasonal Windows	Reference
Sentinel-1	GLCM Entropy	VV_ent, VH_ent	GLCM	Summer/ Winter	[46]
Sentinel-1	GLCM Variance	VV_var, VH_var	GLCM	Summer/ Winter	
Sentinel-1	GLCM Correlation	VV_corr, VH_corr	GLCM	Summer/ Winter	
Sentinel-1	GLCM Contrast	VV_contrast, VH_contrast	GLCM	Summer/ Winter	
Sentinel-2	Chlorophyll Index Red-edge	CIRE	(B8/B5) – 1	Summer/ Autumn	[47]
Sentinel-2	Inverted Red-edge Chlorophyll Index	IRECI	(B8 - B4)/(B5/B6)	Summer/ Autumn	[48]
Sentinel-2	Specific Leaf Area Vegetation Index	SLAVI	B8/(B4 + B12)	Summer/ Autumn	[49]
Sentinel-2	Modified Chlorophyll Absorption in Reflectance Index	MCARI	((B5 - B4) - 0.2 * (B5 - B3)) * (B5/B4)	Summer/ Autumn	[35]
Sentinel-2	Red-edge Normalized Difference Vegetation Index	NDVI705	(B6 - B5)/(B6 + B5)	Summer/ Autumn	[50]
Sentinel-2	Modified Normalized Difference Water Index	MNDWI	(B3 - B11)/(B3 + B11)	Summer/ Autumn	[51]

2.3.4. Seasonal Sentinel-2 Composites

To generate cloud-free seasonal multispectral composites which are ecologically relevant for aspen forests, this study assessed (1) the annual spectral response of aspen reference data (see Sections 2.2.1 and 2.3.2) and (2) the average phenology of aspen forests in the study area. Using these assessments, ecologically relevant time periods were chosen to create median cloud-free image composites.

The annual spectral response was derived using all S2 images available over the study region (see Section 2.3.2). Occluded pixels (e.g., cloud or haze) were identified using the Cloud Score Plus [52] with a threshold value of 0.60. To account for spatial and temporal variations in spectral characteristics, the median bi-weekly surface reflectance was calculated for the aspen presence data over the entire year.

Phenology metrics were summarized from the Visible Infrared Imaging Radiometer Suite (VIIRS) Land Cover Dynamics data product (VNP22Q2), which provides global land surface phenology (GLSP) metrics at yearly intervals [53]. Within the aspen mask (see Section 2.2.1), the median day-of-year for each phenological metric was calculated for each spatial block using the full VIIRS record (2013–2022). Metrics included the onset of greenness increase, onset of greenness decrease, mid-senescence phase, and onset of greenness minimum (see Appendix A for a more detailed description of this data and analysis).

Based on these analyses, this study adopted two ecologically relevant time periods: summer (onset of greenness increase to onset of greenness decrease, 25 May–13 August) and autumn (mid-senescence phase to onset of greenness minimum, 2 September–14 November). For each seasonal period, images with greater than 80% cloud cover and 10% snow cover were excluded. Occluded pixels (e.g., cloud cover, haze) were then masked using the Cloud Score Plus [52] with a threshold for occlusion of 0.60. Composites were created using the median pixel value of all non-occluded pixels across each seasonal period. A total of 3956 S2 tiles were used with per-spatial block averages of 146 (\pm 71) tiles for summer and 73 (\pm 30) tiles for autumn.

Remote Sens. 2024, 16, 1619 9 of 21

2.3.5. Topographic Data

Inclusion of topographic information is shown to improve the accuracy of forest type classifications, especially in regions with complex elevation patterns [35]. Topography was extracted using a digital elevation model (DEM) from the United States Geological Service (USGS) 3-dimensional Elevation Program (3DEP) 1/3 arc-second (10 m) elevation product. From the DEM, slope and aspect were calculated, both of which may influence the distribution of aspen forest cover across the landscape [43].

2.4. Image Classification

In this study, a binary Random Forest (RF) was adopted for classification. RF is a robust machine-learning method which is less sensitive to overfitting while minimizing computational expense associated with large input data [44,54]. A spatial block cross-validation strategy was implemented to account for spatial autocorrelation in the training and validation data [55]. For each fold, a 70:30 ratio was used to randomly split spatial blocks into training and validation sets, respectively. Only presence and background reference data within these splits were used to train the model at each fold. Models were trained with 1001 trees, and the number of random variables used at each split was set to the square root of the number of input variables. To test the relative influence of S1 and S2 data on classification accuracy, model performance was assessed across different classification scenarios (e.g., combinations of season S1 and S2 inputs), and the best-performing combination was selected for classification.

2.4.1. Model Selection and Accuracy Assessment

Model performance was assessed using a set of common metrics based on the confusion matrix for each k-fold model and classification scenario, specifically, the precision, recall, and F1-score. The F1-score was adopted because it typically performs better than overall accuracy in imbalanced classifications [56]. The best-performing classification scenario was selected based on the average F1-score across folds. A feature selection exercise then identified the most parsimonious model for classification to limit multicollinearity. While the predictive ability of RF is likely unaffected by multicollinearity, assessment of feature importance is sensitive to its presence [54]. Tests for multicollinearity were based on the 'multi.collinear' function in the rfUtilities [57] package in the R Statistical Programming Language [58] with a permutated (N = 1001, $p \le 0.05$) leave-one-out method. Features were removed based on the frequency that they were identified in the permutation tests (frequency > 0). Collinear bands included Band 7, Band 8A, and NDVI705 for both summer and autumn, summer Band 8, summer IRECI, and summer MCARI. The 'rf.modelSel' function was then used to identify the most parsimonious set of features based on the out-of-bag error rate to use in the final classification model, thereby improving computation time and minimizing noise [59].

The accuracy of the final model was assessed using the binary classification of the probability surface generated by the RF. Typically, predicted classes are defined based on a single probability threshold between 0 and 1 (e.g., probability > 0.5 belongs to class 1), which may not relate to the optimum classification threshold [55]. The sensitivity to this threshold was tested by calculating the confusion matrix and associated metrics for 100 values between 0 and 1 for each fold. At each threshold in the sequence, the validation data were classified into aspen or non-aspen, and the precision, recall, and F1-score were calculated. We identified the optimal threshold for classification based on the average maximum F1-score across folds (see Appendix B).

2.4.2. Feature Importance

Feature importance was retrieved from the final model, calculated in GEE as the sum of decrease in Gini impurity index over all trees in the forest [60]. Feature importance values for each fold were calculated, and the median values with confidence intervals were extracted.

Remote Sens. **2024**, 16, 1619

2.5. Agreement with Existing Products

Agreement was assessed between the Sentinel-based aspen map and three existing 30 m products: the Landfire EVT (ca. 2016), USFS ITSP (ca. 2014), and USFS TreeMap (ca. 2016). There were two objectives for this assessment: 1—investigate the accuracy of the validation reference data, and 2—test the pixel-based agreement with the Sentinel-based map across the Southern Rockies and the White River NF. Each product was first reclassified into aspen and non-aspen and resampled to a common 10 m spatial resolution to match the Sentinel-based map. For the USFS ITSP and TreeMap, aspen presence was defined using the basal area metric (>10 stems/ha, see Section 2.2.1). For both objectives, the confusion matrix was used to assess agreement using the same metrics (precision, recall, and F1-score). In the case of objective (1), the confusion matrix was based on validation reference data. For objective (2), the confusion matrix is based on all pixels in the study areas with the Sentinel-based map as the reference.

2.6. Case Study: Landscape Patch Dynamics

To highlight the utility of the Sentinel-based map for management activities, this study calculated patch- and class-level landscape metrics across the Southern Rockies and the White River NF. These metrics included landscape (e.g., total area, patch density) and patch (e.g., patch size, perimeter-to-area ratio) statistics. Comparisons of landscape patch dynamics were also made between the existing products. Metrics were calculated using the *pylandstats* Python package [61].

3. Results

3.1. Annual Spectral Response of Quaking Aspen Forests

The annual surface reflectance of quaking aspen forests highlights the patterns of phenology, canopy development, and environmental conditions in the study region (Figure 3A). During winter (December–March), surface reflectance is highly variable as the canopy is in dormancy and stands are often covered in snow, especially at higher elevations. As the canopy develops, a peak in the near-infrared (NIR) and red-edge wavelength occurs around the first week or two of July and corresponds with a mature forest canopy. As the canopy transitions to early autumn, there is a drop in NIR reflectance and an increase in both the visible and shortwave infrared (SWIR), which corresponds to a decrease in green vegetation. A similar pattern is observed for the S2 spectral indices (Figure 3B). The largest difference in reflectance between summer and autumn occurs in the NIR and red-edge regions of the spectrum, although there are significant spectral changes across all S2 bands (Figure 3C) and spectral indices (Figure 3D).

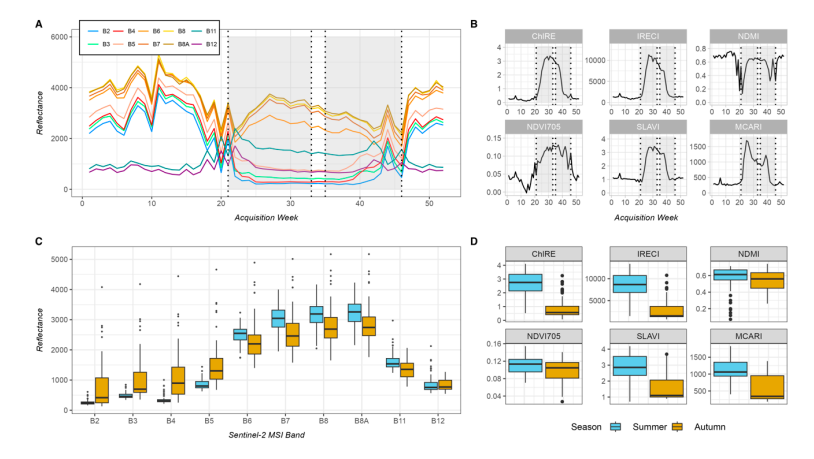


Figure 3. Annual (**A**,**B**) and seasonal (**C**,**D**) spectral response of aspen presence data (ca. 2019). Grey shading defines the temporal windows. (**A**) Median bi-weekly surface reflectance values for S2 bands, (**B**) median weekly response of derived spectral indices, (**C**) seasonal differences in S2 bands from image composites (summer and autumn), (**D**) seasonal difference in spectral indices.

Remote Sens. 2024, 16, 1619 11 of 21

3.2. Model Selection and Accuracy Assessment

The best-performing classification scenario included all features from both S1 and S2 and topographic data with an average F1-score of 0.91 (\pm 0.01, Figure 4). The worst classification scenarios were those in which only S1 data were used (F1-score 0.46–0.62). There was a significant increase in classification accuracy for single-season S2 data (i.e., summer or autumn alone) compared to classifications which used only S1. However, for models which only used S1 as inputs, the addition of GLCM texture features did improve model performance. Combining both seasonal S2 composites and spectral indices increased the average F1-score by 0.3 compared to models which used only one seasonal spectral composite (e.g., only summer or only autumn). The addition of both S1 seasonal composites and texture features only improved the F1-score by 0.1 compared to the model using combined spectral composites. Across all scenarios, there was little variability in accuracy among folds. That is, the classifications were insensitive to different sets of training and validation data used in the spatial block cross-validation.

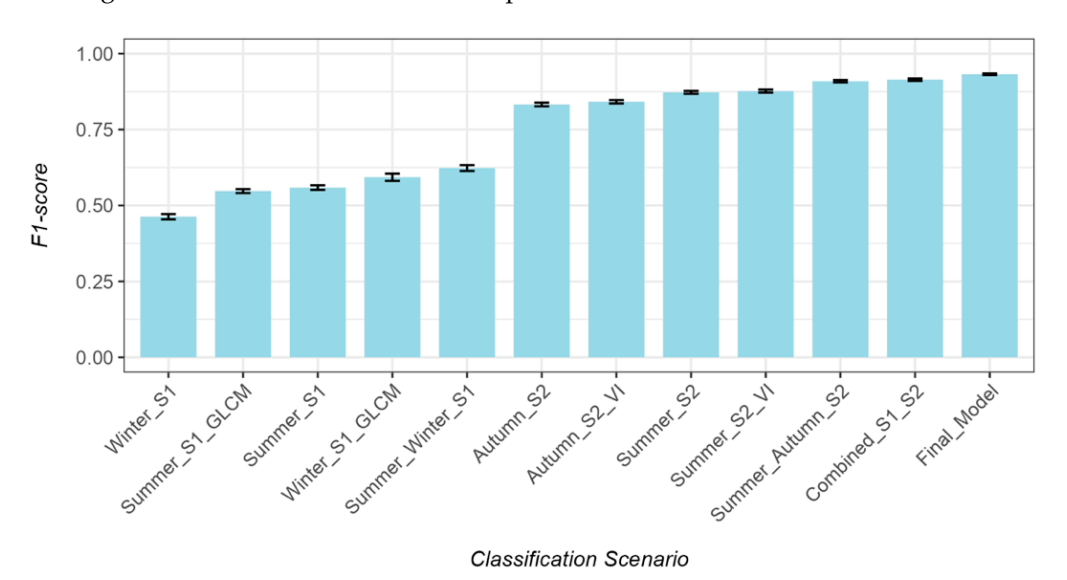


Figure 4. Results from the classification scenarios. We report the average and standard error F1-score across folds for each scenario. Topographic data (elevation, slope, and aspect) were included in all scenarios.

For the best-performing classification scenario ("Combined_S1_S2", Figure 4), which included both S1 and S2 and all texture and spectral indices, a set of 17 bands were selected which minimized the out-of-bag error rate for the most parsimonious classification. Across folds, the final model achieved an average F1-score of 0.931 (± 0.008).

Feature Importance

While there were 17 features in the final model, only the top 10 most important are presented (Figure 5). The Modified Normalized Difference Water Index (MNDWI) from the autumn S2 composite was the top predictor across all folds. Elevation was the second most important feature followed by summer Chlorophyll Index Red-edge (CIRE), autumn Band 3 (green), and the VV polarization band from the summer S1 composite. Just outside of the top five features is the summer Specific Leaf Area Vegetation Index (SLAVI). The remaining features in the top 10 are the red bands for both summer and autumn S2, summer Band 5 (red-edge), and autumn CIRE. Of the 17 bands in the final model, radar textural features were the least important in classifying aspen forests.

Remote Sens. 2024, 16, 1619 12 of 21

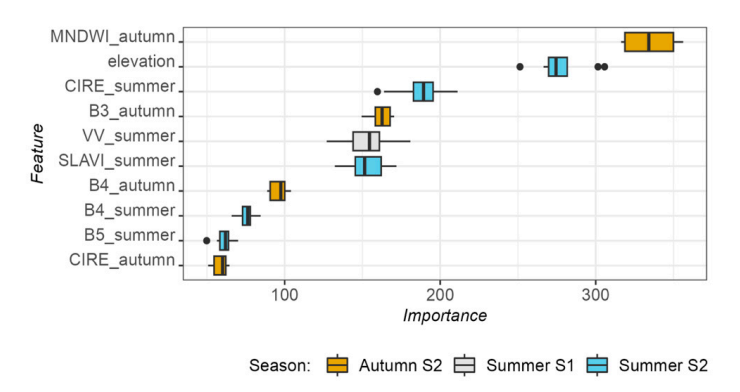


Figure 5. Feature importance for the top 10 features across folds for the final model measured as the sum of decrease in Gini impurity index. Color shade indicates the seasonality.

3.3. Quaking Aspen Forest Map

The resulting high-resolution (10 m) Sentinel-based map of quaking aspen forest cover represents the average probability across folds for the final model (Figure 6D). The optimum probability threshold for classification of 0.42 was identified based on the maximum F1-score achieved across the range of values tested for each fold (Figure A2B). This threshold was used to reclassify the probability map into aspen and non-aspen pixels (Figure 6E). A more detailed description of the threshold and model performance can be found in Appendix B. Across the Southern Rockies, aspen forests cover an estimated 9482 km² (~10.2% of forested area defined by Landfire EVT ca. 2016). In the White River NF (Figure 6B), the Sentinel-based map estimates aspen forest cover extending across 1658 km² (~23.0% of forested area).

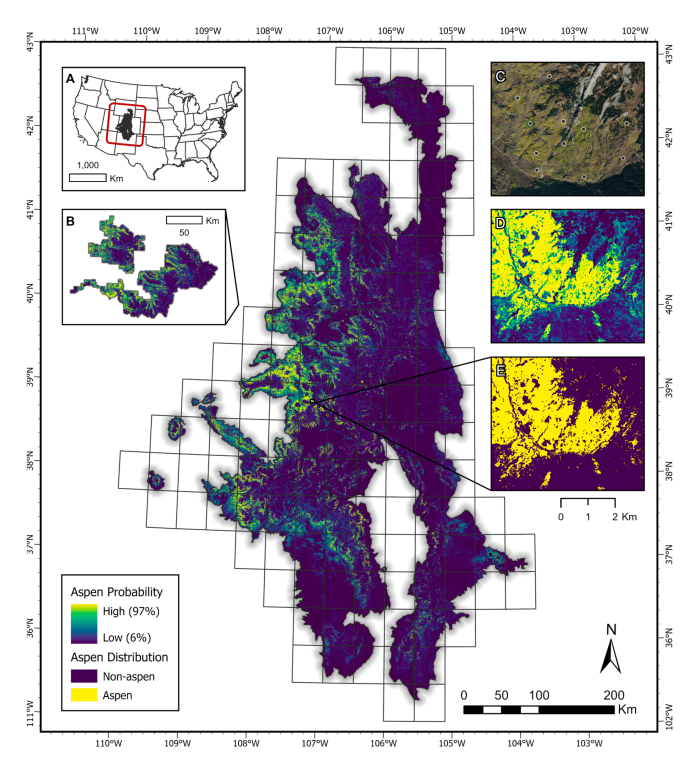


Figure 6. Map of quaking aspen forest cover probability (ca. 2019) for the Southern Rockies, White River NF, and the reference location near Crested Butte, Colorado. (**A**) the location of the Southern Rockies in the western United States (**B**) Inset showing the White River NF and aspen probability map; (**C**) true-color imagery from NAIP (ca. 2017) and aspen reference data for the reference location; (**D**) quaking aspen forest cover probability (%) for the reference location; (**E**) quaking aspen distribution map based on the optimum probability threshold (0.42).

Remote Sens. 2024, 16, 1619 13 of 21

3.4. Agreement with Existing Products

For the first objective (agreement based on validation data), there was strong overall agreement between products with the average F1-score ranging from 0.829 to 0.865 compared to 0.931 for the Sentinel-based map (Table 4). However, a notable pattern emerges regarding precision and recall. The Sentinel-based map demonstrates higher precision (0.9516) relative to recall (0.9116). This suggests that while the map is correctly predicting aspen presence 95% of the time, it may be more restrictive, missing about 9% of true aspen presence. Conversely, all three reference products exhibit lower precision than recall. For example, the USFS TreeMap correctly predicts aspen presence just 80% of the time but identifies 93% of all true aspen presence. This indicates that while existing products are relatively accurate, they may be more likely to include non-aspen areas in their predictions based on the validation reference data.

Table 4. Precision, recall, and F1-score for validation data across three existing products and the Sentinel-based map across the Southern Rockies.

Data Source	Precision	Recall	F1-Score
Sentinel-based map	0.9516	0.9116	0.9311
USFS TreeMap	0.8087	0.9302	0.8652
Landfire EVT	0.8168	0.8995	0.8562
USFS ITSP	0.7959	0.8669	0.8299

For the second objective (pixel-based agreement), there was significant spatial variability in agreement across spatial blocks, with some regions performing significantly better than others (Figure 7). Notably, an opposite relationship emerged between precision and recall in this approach, where precision is consistently higher than recall when comparing existing products to the Sentinel-based map. Given the higher accuracy of the Sentinel-based map based on validation data (Table 4), this supports the finding that existing products may over-predict areas of aspen presence in comparison. Of the three products, the USFS ITSP has the lowest precision and recall based on validation data and the highest precision in pixel-based agreement. This suggests that while there is generally good agreement between aspen presence in the ITSP and the Sentinel-based map (e.g., high pixel-based precision), this product likely overestimates aspen presence on the landscape to a greater degree than the other two products and may also more commonly fail to identify true aspen presence. Additionally, the White River NF exhibits significantly higher precision, recall, and F1-score for all existing products than the median across spatial blocks (Figure 7). This region is characterized by extensive aspen, suggesting that the agreement may be higher in areas with more consistent aspen cover. Still, the higher precision than recall in the pixel-based assessment indicates that there may be overestimation of aspen presence for the three reference products.

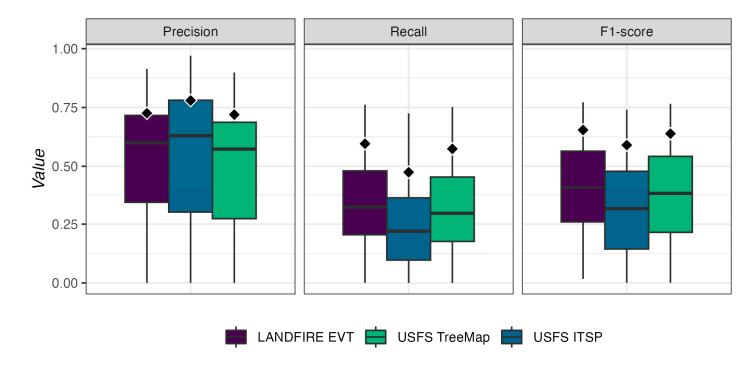


Figure 7. Distribution of pixel-based precision, recall, and F1-score of existing products compared to the Sentinel-based map across spatial blocks within the Southern Rockies. Diamonds indicate the values for the targeted geography (White River NF).

Remote Sens. 2024, 16, 1619 14 of 21

Landscape and Patch Dynamics

The Sentinel-based map estimates 43–118% less total aspen area across the Southern Rockies and 21–64% less in the White River NF compared to existing products (Figure 8A). The average patch size varies greatly across the Southern Rockies, highlighting the regional difference in stand characteristics. For the Sentinel-based map, the average patch size is 0.53 ha (± 23 ha) in the Southern Rockies and 0.74 ha (± 22 ha) in the White River NF, significantly smaller than existing products (Table 5, Figure 8B). Some regions are dominated by large stands of pure aspen (>22 ha), whereas others are defined by many small, more dispersed stands (Figure 8B,C). Notably, the Sentinel-based map identifies 28–93% more individual patches across the Southern Rockies and White River NF. Given the higher accuracy of the Sentinel-based map and the trend in over-prediction of aspen areas from existing products, these results suggest that the higher-resolution map is better able to characterize the actual landscape configuration of aspen forests.

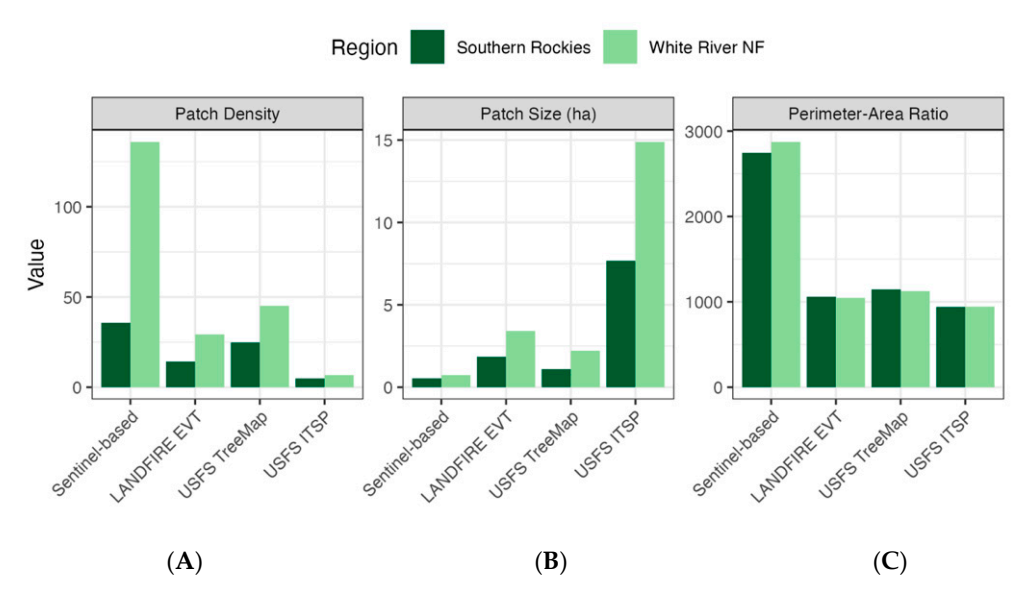


Figure 8. Comparison of patch metrics for the Southern Rockies and the White River NF for the Sentinel-based map and the three existing products. The White River NF is dominated by large, often pure stands of quaking aspen, which is highlighted in the much larger average patch density and patch size when compared to the Southern Rockies (A–C).

Table 5. Landscape patch dynamics summarized across spatial blocks for the Southern Rockies. We report the total area, number of patches, average patch density, average patch size, and average perimeter-to-area ratio.

Data Source	Total Area (km²)	Number of Patches	Patch Density	Average Patch Size (ha)	Average Perimeter/ Area Ratio
Sentinel-based Map	9384.41	1,760,386	35.73	0.53	2745.57
Landfire EVT	13,441.59	728,370	14.22	1.85	1060.98
USFS TreeMap	13,931.85	1,268,131	24.82	1.10	1145.88
USFS ITSP	20,477.69	266,762	4.82	7.68	941.75

4. Discussion

This overall effort provides a new high-resolution (10 m), accurate (0.93 mean F1-score) aspen forest cover map for the Southern Rockies (ca. 2019) and reproducible methods for extending this analysis in other regions, over time, or for other species of interest. Leveraging GEE for data acquisition and analysis, aspen forests were mapped across a large geographic region (~130k km²) using over 5000 images from Sentinel-1 and Sentinel-2. Aspen forests were found to cover 9482 km² (~10.2% of forested area) in the Southern Rockies and 1658 km² (~23.0% of forested area) in the White River NF. This new map offers

Remote Sens. 2024, 16, 1619 15 of 21

improvements over existing products both in terms of accuracy (0.07–0.17 higher F1-score based on comparison with the validation reference data) and identification of smaller forest patches (1.3–7.2 ha smaller average patch size). Furthermore, this study importantly demonstrates the utility of two methodological choices for forest species identification using satellite data. First, integrating species- and location-specific phenology metrics help create ecologically relevant multispectral image composites over large and environmentally diverse regions. Classification performance was greatly enhanced when combining at least two seasonal composites and spectral indices compared to models which used only radar and derived textural features. Second, binary RF and spatial block cross-validation provide efficient tools for training and assessing classification tasks using remote-sensing imagery, especially across large geographic areas. Future large-area and species-specific image classification research may benefit from the methods described in the present study.

Previous studies have shown the effectiveness of multi-temporal S2 imagery for improving classification accuracy of forest species, especially in heterogeneous environments, e.g., [29-31,62]. For example, Persson et al. [31] demonstrated that the successive addition of S2 image dates increased the overall accuracy of forest type identification in Sweden. Similarly, Grabska et al. [63] showed the improved classification accuracy when at least two S2 image dates were used in classification of forest species in Poland. Consistent with these findings, the present study achieves higher classification accuracy when combining multiple seasonal composites compared to just a single season. Furthermore, incorporating phenology difference in species identification tasks using S2 may improve accuracy. The study by Li et al. [29] demonstrated that incorporating species phenology and multitemporal S2 imagery produced accurate maps of *Populus euphratica* distribution. However, this study, like many referenced here, used a single S2 tile for classification. Large-area image classification, especially in heterogenous landscapes, introduces challenges for incorporating phenology. Our study demonstrates that using landscape-scale phenology from coarse-resolution satellite data (e.g., VIIRS) can help identify temporal periods that relate to key phenological stages for a deciduous forest species. Given the availability of VIIRS data globally, these methods could be used in other parts of the world for species with distinct phenological patterns. In addition, the finding that classification using only S1 features poorly identifies aspen forests compared to classifications which use S2 or a combination of S1 and S2 is also consistent with previous research. For example, Dobrinić et al. [35] found that using only S1 features in the classification of vegetation type in northern Croatia yielded a 75% overall accuracy compared to 92% when combining S1 and S2. While some previous research indicates the effectiveness of GLCM texture for vegetation mapping, e.g., [34,35], our results indicate minimal influence of these features on classification accuracy of aspen presence. Despite these results, there is some evidence of a correlation between radar backscatter and aspen forest cover as indicated by the presence of the summer VV band in the top five most influential features in the final model. Future research should explore this relationship more and may benefit from investigating different pixel neighborhood sizes for GLCM texture features or other indices derived from radar data at different times of the year.

In the western United States, quaking aspen is the dominant deciduous forest type in an otherwise conifer-dominated landscape. Aspen forests contain higher levels of canopy moisture content compared to their conifer neighbors [63]. This study demonstrated that spectral indices derived from S2 which leverage the red-edge and SWIR bands to estimate canopy moisture and chlorophyl content are important features for classification. For example, two of the most important features in the final model were the Modified Normalized Water Index (MNDWI) and the Chlorophyl Red-edge Index (CIRE) for the summer image composite. Leveraging unique canopy characteristics to create targeted spectral indices may improve forest species mapping, particularly deciduous species. However, more work is needed to understand if this relationship is maintained in other regions of the world and in different environmental conditions, especially in areas with more diversity of deciduous forest species.

Remote Sens. **2024**, 16, 1619

While the present study achieved high classification accuracy at a finer spatial resolution than existing products, several limitations and areas for future research exist. First, the relatively short observational record precludes mapping efforts prior to 2015 using S1 or S2. Second, although the spatial resolution of Sentinel is better than other similar multispectral satellite imagery (e.g., Landsat), the map produced in the present study may still miss detections of small stands or where aspen is intermixed with conifer species in the canopy (e.g., seral aspen). As the availability of very-high-resolution satellite imagery increases (e.g., the CBERS-4 mission), efforts should be made to improve on the detection of small stands. Analysis techniques such as spectral unmixing may also prove useful for mapping intermixed conifer-aspen stands with very-high-spatial-resolution imagery. Third, the lack of field-based training and validation data in the current study is a major limitation. Although this challenge was partially overcome by using photo interpretation, future efforts should focus on integrating field measurements to improve the reliability and assessment of model performance. By investigating accuracy and agreement with other products across space, the present study identifies areas where performance may be low. In these areas, development of more precise training and validation data may improve the overall ability of the model to distinguish aspen forests from other cover types. Collecting data from existing field studies, citizen science databases (e.g., iNaturalist), or species occurrence databases (e.g., the Global Biodiversity Information Facility) may provide additional accuracy assessment and model improvements while limiting the need for time-intensive photo interpretation efforts and extensive field campaigns. Future efforts may also include more state-of-the-art classification techniques such as neural networks and object-oriented classification, which would take advantage of the spatial characteristics of aspen stands. Moreover, the use of upcoming hyperspectral imaging campaigns (e.g., EMIT) or satellite-based LiDAR (e.g., GEDI) will undoubtedly offer continued improvements to forest species mapping.

Despite these limitations, this study provides a crucial tool for land managers in determining where to prioritize active management of aspen forests. Quaking aspen is a shade-intolerant species capable of vegetation regeneration from root suckers; as such, it readily occupies canopy openings [7,15]. These characteristics have been used to regenerate and even expand aspen patches using coppice silviculture techniques or prescribed fire, where appropriate [15]. Furthermore, the landscape dynamics of aspen vary across the Southern Rockies, with some areas dominated by pure or stable stands and others characterized by mid–late successional seral stands [4,13]. These different functional types respond to different management practices. The improved capability to map aspen forest patches at finer spatial resolution and high accuracy is useful for forest managers who are planning silvicultural management activities which maximize the potential for expansion of aspen into new areas. Combined with other datasets including habitat suitability, wildfire or other disturbance risk, and others, these new maps have the potential to assist forest management at both temporal and spatial scales relevant to the ecology of the species.

5. Conclusions

This study contributes to the broader challenges of forest species identification from remotely sensed imagery across large geographic areas. Using broad-scale temporal and spatial data, quaking aspen was identified, and a finer-resolution aspen distribution map was created across the Southern Rockies. By leveraging species-specific phenology based on observational data, our study provides a method for generating ecologically relevant seasonal imagery composites for a species of interest. This is particularly useful for applications using multispectral imagery in which scenes are often occluded by cloud or atmospheric haze, especially in regions of the world with persistent cloud cover or complex topography. These methods can be applied globally for various species of interest with distinct phenology. Furthermore, the application of spatial block cross-validation and Random Forests in GEE demonstrates an effective and accurate method for handling large data analysis in a cloud-computing environment. The methods are fully open, providing

Remote Sens. 2024, 16, 1619 17 of 21

the research community with important references to replicate this study in other regions of the world.

As human- and climate-related impacts to forested areas continue to grow, the development of new high-resolution and accurate maps of forest species is critical to effective management activities which improve resilience, reduce hazard for communities, and maintain important ecosystem service benefits. Given the uncertainty around aspen growth dynamics in a changing climate, this product is an important source of information for forest managers and will benefit management of one of the most widely distributed tree species in North America.

Author Contributions: Conceptualization, M.C., T.C., S.H. and J.B.; methodology, M.C. and T.C.; software, M.C.; formal analysis, M.C.; investigation, M.C. and T.C.; data curation, M.C.; writing—original draft preparation, M.C.; writing—review and editing, M.C., T.C., S.H., A.P. and J.B.; visualization, M.C.; supervision, S.H. and J.B.; project administration, S.H. and J.B.; funding acquisition, S.H., J.B. and M.C. All authors have read and agreed to the published version of the manuscript.

Funding: This research was funded by the Joint Fire Science Program (JFSP, Project ID 21-2-02-29).

Data Availability Statement: Data associated with this paper are available as public Google Earth Engine assets. An interactive web viewing application provides access to the results and input satellite data (https://maco.users.earthengine.app/view/aspen-viewer (accessed on 31 March 2024)). All analyses and code used in this paper are available in a public GitHub repository (https://github.com/maxwellCcook/aspen-fire (accessed on 31 March 2024)) and a public Google Earth Engine repository (https://code.earthengine.google.com/?accept_repo=users/maco/aspen-fire (accessed on 31 March 2024)).

Acknowledgments: Support from the Earth Lab, Cooperative Institute for Research in Environmental Science (CIRES), Department of Geography University of Colorado Boulder, and the Department of Forest and Rangeland Stewardship Colorado State University. The authors would like to acknowledge Cibele Do Amaral, Catherine Schloegel, and Kyle Rodman for their intellectual contributions and for discussions related to the manuscript and undergraduate research assistant Adam Thomas for his dedicated work towards developing the aspen presence data.

Conflicts of Interest: The authors declare no conflicts of interest. The funders had no role in the design of the study; in the collection, analyses, or interpretation of data; in the writing of the manuscript; or in the decision to publish the results.

Appendix A. Phenology of Quaking Aspen across the Southern Rockies

The Southern Rockies study region is an ecologically diverse landscape with complex topography. In complex systems, exploring the phenological patterns of vegetation development is useful when generating seasonal satellite image composites [27]. For quaking aspen forests in particular, the timing of canopy growth differs by elevation, slope, and climate [64]. These differences across a large and diverse region can influence the generation of satellite image composites which are representative of specific phenological stages for this deciduous forest species.

To examine the seasonal variation of canopy development within aspen forests across the Southern Rockies, we summarized phenological metrics from the Visible Infrared Imaging Radiometer Suite (VIIRS) Land Cover Dynamics data product (VNP22Q2), which provides global land surface phenology metrics at yearly intervals since 2013 [53]. These include day-of-year (DOY) for the onset of greenness increase, mid-greenup phase, onset of greenness maximum, onset of greenness decrease, mid-senescence phase, and the onset of greenness minimum. For each spatial block, we calculated the median day-of-year for each metric within aspen forest area based on the USFS TreeMap product (see Section 2.2.1 of the main text). Analysis was carried out in the Google Earth Engine (GEE) Code Editor [21]. We examined the variation in the average DOY across spatial blocks (Figure A1) for each metric and calculated the average and standard deviation across blocks and years for the Southern Rockies. The variation in quaking aspen phenology is well-explained by elevation as demonstrated by the inset plots in Figure A1. To capture this variation when selecting

Remote Sens. 2024, 16, 1619 18 of 21

temporal windows for creating seasonal image composites, we subtracted the standard deviation (in days) from the metric average (day-of-year) and used these values as start and end dates. Specifically, we defined two temporal windows: summer, or the mid-greenup phase to the onset of greenness decrease; and autumn, or the mid-senescence phase to the onset of greenness minimum.

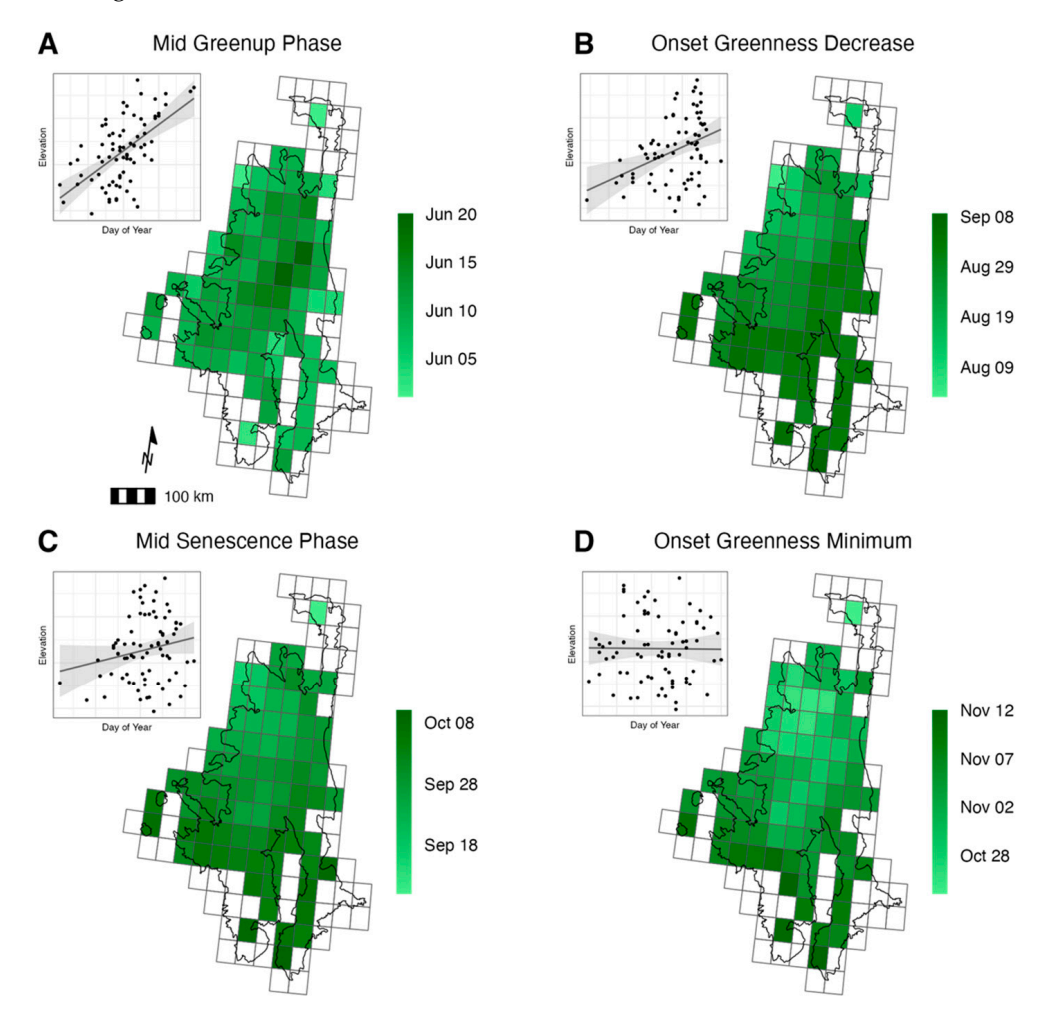


Figure A1. Quaking aspen phenology derived from the VNP22Q1 in the Southern Rockies and relationship with elevation. Day-of-year estimates represent the median across all years (2013–2022). **(A)** Mid-greenup phase (late May to late June) and **(B)** the onset of greenness decrease (early August to early September) defines the summer temporal window, and both show a strong positive linear relationship with elevation. **(C)** Mid-senescence phase (mid-September to early October) and **(D)** the onset of greenness minimum (late October to mid-November) define the autumn temporal window. Senescence phase indicates a strong relationship with elevation while the onset of greenness minimum is less influenced by elevation.

Appendix B. Accuracy Assessment and Optimal Threshold for Classification

To assess model performance and to calculate the optimum threshold for classification based on the probability grids from the Random Forest classifier, we calculated a confusion matrix for 100 different classification threshold values between 0 and 1 based on the training data in each of the 10 model iterations. From this, we calculated an AUC-ROC curve which represents the true positive rate against the false positive rate (Figure A2A). To calculate the optimum threshold, we found the maximum F1-score of the average across all 10 model iterations (Figure A2B). We used this optimum threshold on the average probability of aspen forest grid to calculate the aspen distribution map (aspen and no aspen).

Remote Sens. 2024, 16, 1619 19 of 21

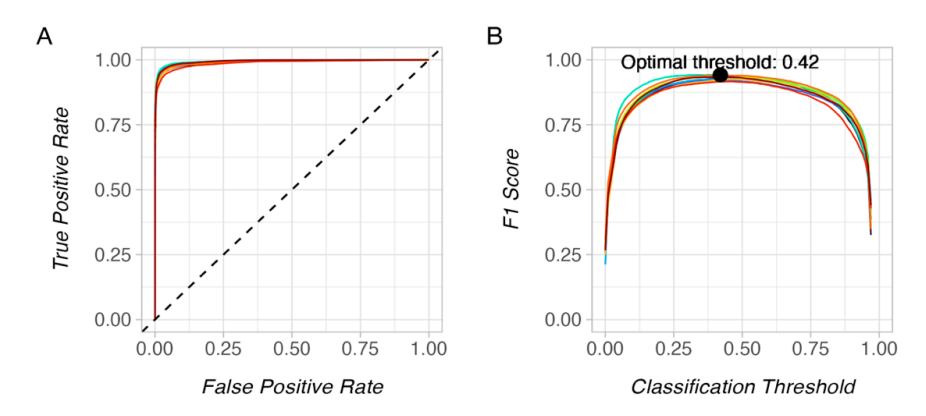


Figure A2. Model performance metrics from the final classification. **(A)** AUC-ROC or the true-positive rate against the false-positive rate with colors representing the 10 model iterations; **(B)** the F1-score across threshold values. The black line is the average across model iterations, and the black point represents the location of the maximum F1 from the average across folds. This point is our optimum threshold for classification (0.42).

References

- Rogers, P.C.; Pinno, B.D.; Šebesta, J.; Albrectsen, B.R.; Li, G.; Ivanova, N.; Kusbach, A.; Kuuluvainen, T.; Landhäusser, S.M.; Liu, H.; et al. A Global View of Aspen: Conservation Science for Widespread Keystone Systems. *Glob. Ecol. Conserv.* 2020, 21, e00828. [CrossRef]
- 2. Debyle, N.V.; Winokur, R.P. Aspen: Ecology and Management in the Western United States. General Technical Report RM-119, USDA Forest Service. 1985. Available online: https://www.academia.edu/34572963/Aspen_ecology_and_management_in_the_western_United_States (accessed on 31 March 2024).
- 3. Bartos, D.L. Landscape dynamics of aspen and conifer forests. In *Sustaining Aspen in Western Landscapes: Symposium Proceedings;* Shepperd, W.D., Binkley, D., Bartos, D.L., Stohlgren, T.J., Eskew, L.G., Eds.; Proceedings RMRS-P-18; U.S. Department of Agriculture, Forest Service, Rocky Mountain Research Station: Fort Collins, CO, USA, 2001.
- 4. Rogers, P.C.; Landhäusser, S.M.; Pinno, B.D.; Ryel, R.J. A Functional Framework for Improved Management of Western North American Aspen (*Populus Tremuloides* Michx.). For. Sci. 2014, 60, 345–359. [CrossRef]
- 5. Landhäusser, S.M.; Deshaies, D.; Lieffers, V.J. Disturbance Facilitates Rapid Range Expansion of Aspen into Higher Elevations of the Rocky Mountains under a Warming Climate. *J. Biogeogr.* **2010**, *37*, 68–76. [CrossRef]
- 6. Gill, N.S.; Sangermano, F.; Buma, B.; Kulakowski, D. Populus Tremuloides Seedling Establishment: An Underexplored Vector for Forest Type Conversion after Multiple Disturbances. *For. Ecol. Manag.* **2017**, *404*, 156–164. [CrossRef]
- 7. Long, J.N.; Mock, K. Changing Perspectives on Regeneration Ecology and Genetic Diversity in Western Quaking Aspen: Implications for Silviculture. *Can. J. For. Res.* **2012**, *42*, 2011–2021. [CrossRef]
- 8. Andrus, R.A.; Hart, S.J.; Tutland, N.; Veblen, T.T. Future Dominance by Quaking Aspen Expected Following Short-Interval, Compounded Disturbance Interaction. *Ecosphere* **2021**, *12*, e03345. [CrossRef]
- 9. Nigro, K.M.; Rocca, M.E.; Battaglia, M.A.; Coop, J.D.; Redmond, M.D. Wildfire Catalyzes Upward Range Expansion of Trembling Aspen in Southern Rocky Mountain Beetle-Killed Forests. *J. Biogeogr.* **2022**, *49*, 201–214. [CrossRef]
- 10. Worrall, J.J.; Rehfeldt, G.E.; Hamann, A.; Hogg, E.H.; Marchetti, S.B.; Michaelian, M.; Gray, L.K. Recent Declines of Populus Tremuloides in North America Linked to Climate. *For. Ecol. Manag.* **2013**, 299, 35–51. [CrossRef]
- 11. Rosenblum, A. Altered Fire Regimes and the Persistence of Quaking Aspen in the Rocky Mountains: A Literature Review. *Open J. For.* **2015**, *5*, 563–567. [CrossRef]
- 12. Krasnow, K.D.; Stephens, S.L. Evolving Paradigms of Aspen Ecology and Management: Impacts of Stand Condition and Fire Severity on Vegetation Dynamics. *Ecosphere* **2015**, *6*, 1–16. [CrossRef]
- 13. Shinneman, D.J.; McIlroy, S.K. Climate and Disturbance Influence Self-Sustaining Stand Dynamics of Aspen (Populus Tremuloides) near Its Range Margin. *Ecol. Appl.* **2019**, 29, e01948. [CrossRef] [PubMed]
- 14. Picotte, J.J.; Dockter, D.; Long, J.; Tolk, B.; Davidson, A.; Peterson, B. LANDFIRE Remap Prototype Mapping Effort: Developing a New Framework for Mapping Vegetation Classification, Change, and Structure. *Fire* **2019**, *2*, 35. [CrossRef]
- 15. Shepperd, W.D.; Smith, F.W.; Pelz, K.A. Group Clearfell Harvest Can Promote Regeneration of Aspen Forests Affected by Sudden Aspen Decline in Western Colorado. *For. Sci.* **2015**, *61*, 932–937. [CrossRef]
- 16. Landhäusser, S.M.; Pinno, B.D.; Mock, K.E. Tamm Review: Seedling-Based Ecology, Management, and Restoration in Aspen (*Populus Tremuloides*). For. Ecol. Manag. **2019**, 432, 231–245. [CrossRef]
- 17. Ellenwood, J.R.; Krist, F.J.; Romero, S.A. *National Individual Tree Species Atlas*; FHTET-15–01; USDA Forest Service, Forest Health Technology Enterprise Team: Fort Collins, CO, USA, 2015. Available online: https://www.fs.usda.gov/foresthealth/applied-sciences/mapping-reporting/indiv-tree-parameter-maps.shtml (accessed on 31 March 2024).

Remote Sens. **2024**, 16, 1619

18. Riley, K.L.; Grenfell, I.C.; Shaw, J.D.; Finney, M.A. TreeMap 2016 Dataset Generates CONUS-Wide Maps of Forest Characteristics Including Live Basal Area, Aboveground Carbon, and Number of Trees per Acre. *J. For.* 2022, 120, 607–632. [CrossRef]

- 19. Landfire. Landfire (LF) 2016 Remap EVT Agreement Assessment. Available online: https://landfire.gov/remapevt_assessment. php (accessed on 31 March 2024).
- 20. Hermosilla, T.; Wulder, M.A.; White, J.C.; Coops, N.C. Land Cover Classification in an Era of Big and Open Data: Optimizing Localized Implementation and Training Data Selection to Improve Mapping Outcomes. *Remote Sens. Environ.* **2022**, *268*, 112780. [CrossRef]
- 21. Gorelick, N.; Hancher, M.; Dixon, M.; Ilyushchenko, S.; Thau, D.; Moore, R. Google Earth Engine: Planetary-Scale Geospatial Analysis for Everyone. *Remote Sens. Environ.* **2017**, 202, 18–27. [CrossRef]
- 22. Phiri, D.; Simwanda, M.; Salekin, S.; Nyirenda, V.R.; Murayama, Y.; Ranagalage, M. Sentinel-2 Data for Land Cover/Use Mapping: A Review. *Remote Sens.* **2020**, *12*, 2291. [CrossRef]
- 23. Bayle, A.; Carlson, B.Z.; Thierion, V.; Isenmann, M.; Choler, P. Improved Mapping of Mountain Shrublands Using the Sentinel-2 Red-Edge Band. *Remote Sens.* **2019**, *11*, 2807. [CrossRef]
- 24. Clevers, J.G.P.W.; Gitelson, A. Using the Red-Edge Bands on Sentinel-2 for Retrieving Canopy Chlorophyll and Nitrogen Content. In Proceedings of the European Space Agency, Frascati, Italy, 23–27 April 2012. (Special Publication) 2012; Volume ESA SP 707.
- 25. Lin, S.; Li, J.; Liu, Q.; Li, L.; Zhao, J.; Yu, W. Evaluating the Effectiveness of Using Vegetation Indices Based on Red-Edge Reflectance from Sentinel-2 to Estimate Gross Primary Productivity. *Remote Sens.* **2019**, *11*, 1303. [CrossRef]
- 26. Wong, C.Y.S.; D'Odorico, P.; Bhathena, Y.; Arain, M.A.; Ensminger, I. Carotenoid Based Vegetation Indices for Accurate Monitoring of the Phenology of Photosynthesis at the Leaf-Scale in Deciduous and Evergreen Trees. *Remote Sens. Environ.* **2019**, 233, 111407. [CrossRef]
- 27. Kollert, A.; Bremer, M.; Löw, M.; Rutzinger, M. Exploring the Potential of Land Surface Phenology and Seasonal Cloud Free Composites of One Year of Sentinel-2 Imagery for Tree Species Mapping in a Mountainous Region. *Int. J. Appl. Earth Obs. Geoinf.* **2021**, *94*, 102208. [CrossRef]
- 28. Immitzer, M.; Neuwirth, M.; Böck, S.; Brenner, H.; Vuolo, F.; Atzberger, C. Optimal Input Features for Tree Species Classification in Central Europe Based on Multi-Temporal Sentinel-2 Data. *Remote Sens.* **2019**, *11*, 2599. [CrossRef]
- 29. Li, H.; Shi, Q.; Wan, Y.; Shi, H.; Imin, B. Using Sentinel-2 Images to Map the Populus Euphratica Distribution Based on the Spectral Difference Acquired at the Key Phenological Stage. *Forests* **2021**, *12*, 147. [CrossRef]
- 30. Macintyre, P.; van Niekerk, A.; Mucina, L. Efficacy of Multi-Season Sentinel-2 Imagery for Compositional Vegetation Classification. *Int. J. Appl. Earth Obs. Geoinf.* **2020**, *85*, 101980. [CrossRef]
- 31. Persson, M.; Lindberg, E.; Reese, H. Tree Species Classification with Multi-Temporal Sentinel-2 Data. *Remote Sens.* **2018**, *10*, 1794. [CrossRef]
- 32. Barber, B.C. Review Article. Theory of Digital Imaging from Orbital Synthetic-Aperture Radar. *Int. J. Remote Sens.* **1985**, *6*, 1009–1057. [CrossRef]
- 33. Udali, A.; Lingua, E.; Persson, H.J. Assessing Forest Type and Tree Species Classification Using Sentinel-1 C-Band SAR Data in Southern Sweden. *Remote Sens.* **2021**, *13*, 3237. [CrossRef]
- 34. Numbisi, F.N.; Numbisi, F.N.; Coillie, F.V.; Wulf, R.D. Multi-date sentinel1 sar image textures discriminate perennial agroforests in a tropical forest-savannah transition landscape. *Int. Arch. Photogramm. Remote Sens. Spat. Inf. Sci.* **2018**, XLII–1, 339–346. [CrossRef]
- 35. Dobrinić, D.; Gašparović, M.; Medak, D. Sentinel-1 and 2 Time-Series for Vegetation Mapping Using Random Forest Classification: A Case Study of Northern Croatia. *Remote Sens.* **2021**, *13*, 2321. [CrossRef]
- 36. Lechner, M.; Dostálová, A.; Hollaus, M.; Atzberger, C.; Immitzer, M. Combination of Sentinel-1 and Sentinel-2 Data for Tree Species Classification in a Central European Biosphere Reserve. *Remote Sens.* **2022**, *14*, 2687. [CrossRef]
- 37. Liu, Y.; Gong, W.; Hu, X.; Gong, J. Forest Type Identification with Random Forest Using Sentinel-1A, Sentinel-2A, Multi-Temporal Landsat-8 and DEM Data. *Remote Sens.* **2018**, *10*, 946. [CrossRef]
- 38. Steinhausen, M.J.; Wagner, P.D.; Narasimhan, B.; Waske, B. Combining Sentinel-1 and Sentinel-2 Data for Improved Land Use and Land Cover Mapping of Monsoon Regions. *Int. J. Appl. Earth Obs. Geoinf.* **2018**, *73*, 595–604. [CrossRef]
- 39. Dusseux, P.; Corpetti, T.; Hubert-Moy, L.; Corgne, S. Combined Use of Multi-Temporal Optical and Radar Satellite Images for Grassland Monitoring. *Remote Sens.* **2014**, *6*, 6163–6182. [CrossRef]
- 40. Haralick, R.M.; Shanmugam, K.; Dinstein, I. Textural Features for Image Classification. *IEEE Trans. Syst. Man Cybern.* **1973**, *SMC-3*, 610–621. [CrossRef]
- 41. Johnson, R.M. Help Build the Protected Areas Database of the United States (PAD-US); Fact Sheet: Reston, VA, USA, 2023.
- 42. Peete, R.K. Forest and Meadows of the Rocky Mountains. In *North American Terrestrial Vegetation*; Cambridge University Press: New York, NY, USA, 1988; pp. 63–102.
- 43. Shepperd, W. A Classification of Quaking Aspen in the Central Rocky Mountains Based on Growth and Stand Characteristics. *West. J. Appl. For.* **1990**, *5*, 69–75. [CrossRef]
- 44. Deng, X.; Li, W.; Liu, X.; Guo, Q.; Newsam, S. One-Class Remote Sensing Classification: One-Class vs. Binary Classifiers. *Int. J. Remote Sens.* **2018**, 39, 1890–1910. [CrossRef]
- 45. Mullissa, A.; Vollrath, A.; Odongo-Braun, C.; Slagter, B.; Balling, J.; Gou, Y.; Gorelick, N.; Reiche, J. Sentinel-1 SAR Backscatter Analysis Ready Data Preparation in Google Earth Engine. *Remote Sens.* **2021**, *13*, 1954. [CrossRef]

Remote Sens. **2024**, 16, 1619

46. Farwell, L.S.; Gudex-Cross, D.; Anise, I.E.; Bosch, M.J.; Olah, A.M.; Radeloff, V.C.; Razenkova, E.; Rogova, N.; Silveira, E.M.O.; Smith, M.M.; et al. Satellite Image Texture Captures Vegetation Heterogeneity and Explains Patterns of Bird Richness. *Remote Sens. Environ.* **2021**, 253, 112175. [CrossRef]

- 47. Gitelson, A.A.; Gritz, Y.; Merzlyak, M.N. Relationships between Leaf Chlorophyll Content and Spectral Reflectance and Algorithms for Non-Destructive Chlorophyll Assessment in Higher Plant Leaves. *J. Plant Physiol.* **2003**, *160*, 271–282. [CrossRef]
- 48. Frampton, W.J.; Dash, J.; Watmough, G.; Milton, E.J. Evaluating the Capabilities of Sentinel-2 for Quantitative Estimation of Biophysical Variables in Vegetation. *ISPRS J. Photogramm. Remote Sens.* **2013**, *82*, 83–92. [CrossRef]
- 49. Kobayashi, N.; Tani, H.; Wang, X.; Sonobe, R. Crop Classification Using Spectral Indices Derived from Sentinel-2A Imagery. *J. Inf. Telecommun.* **2020**, *4*, 67–90. [CrossRef]
- 50. Evangelides, C.; Nobajas, A. Red-Edge Normalised Difference Vegetation Index (NDVI705) from Sentinel-2 Imagery to Assess Post-Fire Regeneration. *Remote Sens. Appl. Soc. Environ.* **2020**, *17*, 100283. [CrossRef]
- 51. Jiang, W.; Ni, Y.; Pang, Z.; He, G.; Fu, J.; Lu, J.; Yang, K.; Long, T.; Lei, T. A new index for identifying water body from sentinel-2 satellite remote sensing imagery. *ISPRS Ann. Photogramm. Remote Sens. Spat. Inf. Sci.* **2020**, *V-3*–2020, 33–38. [CrossRef]
- 52. Pasquarella, V.J.; Brown, C.F.; Czerwinski, W.; Rucklidge, W.J. Comprehensive Quality Assessment of Optical Satellite Imagery Using Weakly Supervised Video Learning. In Proceedings of the 2023 IEEE/CVF Conference on Computer Vision and Pattern Recognition Workshops (CVPRW), Vancouver, BC, Canada, 17–24 June 2023; pp. 2125–2135.
- 53. Zhang, X.; Liu, L.; Liu, Y.; Jayavelu, S.; Wang, J.; Moon, M.; Henebry, G.M.; Friedl, M.A.; Schaaf, C.B. Generation and Evaluation of the VIIRS Land Surface Phenology Product. *Remote Sens. Environ.* **2018**, 216, 212–229. [CrossRef]
- 54. Belgiu, M.; Drăgut, L. Random Forest in Remote Sensing: A Review of Applications and Future Directions. *ISPRS J. Photogramm. Remote Sens.* **2016**, 114, 24–31. [CrossRef]
- 55. Karasiak, N.; Dejoux, J.-F.; Monteil, C.; Sheeren, D. Spatial Dependence between Training and Test Sets: Another Pitfall of Classification Accuracy Assessment in Remote Sensing. *Mach. Learn.* **2021**, 111, 2715–2740. [CrossRef]
- 56. Uhl, J.H.; Leyk, S. A Framework for Scale-Sensitive, Spatially Explicit Accuracy Assessment of Binary Built-up Surface Layers. *Remote Sens. Environ.* **2022**, 279, 113117. [CrossRef]
- 57. Evans, J.S.; Murphy, M.A. rfUtilities. 2018. Available online: https://github.com/jeffreyevans/rfUtilities (accessed on 31 March 2024).
- 58. R Core Team. R: A Language and Environment for Statistical Computing; R Foundation for Statistical Computing: Vienna, Austria, 2022.
- 59. Evans, J.S.; Cushman, S.A. Gradient Modeling of Conifer Species Using Random Forests. *Landsc. Ecol.* **2009**, 24, 673–683. [CrossRef]
- 60. Nembrini, S.; König, I.R.; Wright, M.N. The Revival of the Gini Importance? Bioinformatics 2018, 34, 3711–3718. [CrossRef]
- 61. Bosch, M. PyLandStats: An Open-Source Pythonic Library to Compute Landscape Metrics. *PLoS ONE* **2019**, *14*, e0225734. [CrossRef] [PubMed]
- 62. Shinneman, D.J.; Baker, W.L.; Rogers, P.C.; Kulakowski, D. Fire Regimes of Quaking Aspen in the Mountain West. *For. Ecol. Manag.* **2013**, 299, 22–34. [CrossRef]
- 63. Grabska, E.; Hostert, P.; Pflugmacher, D.; Ostapowicz, K. Forest Stand Species Mapping Using the Sentinel-2 Time Series. *Remote Sens.* **2019**, *11*, 1197. [CrossRef]
- 64. Meier, G.A.; Brown, J.F.; Evelsizer, R.J.; Vogelmann, J.E. Phenology and Climate Relationships in Aspen (Populus Tremuloides Michx.) Forest and Woodland Communities of Southwestern Colorado. *Ecol. Indic.* **2015**, *48*, 189–197. [CrossRef]

Disclaimer/Publisher's Note: The statements, opinions and data contained in all publications are solely those of the individual author(s) and contributor(s) and not of MDPI and/or the editor(s). MDPI and/or the editor(s) disclaim responsibility for any injury to people or property resulting from any ideas, methods, instructions or products referred to in the content.